Computational studies of electronic circular dichroism spectra predict absolute configuration assignments for the guanine oxidation product 5-carboxamido-5-formamido-2-iminohydantoin†

Aaron M. Fleming,[a] Omar Alshykhly,[a] Anita M. Orendt,[a,b] and Cynthia J. Burrows[a]*

[a]Department of Chemistry, University of Utah, 315 South 1400 East, Salt Lake City, Utah 84112-0850, USA

[b]Center for High Performance Computing, University of Utah, Salt Lake City, Utah 84112-0190, USA

*To whom correspondence should be addressed.

Phone: (801) 585-7290 E-mail: burrows@chem.utah.edu

TOC Graphic

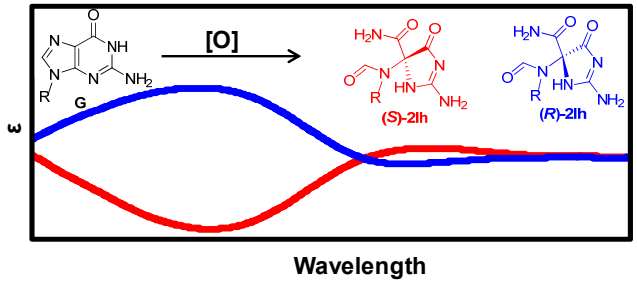

†Dedicated to the memory of Professor Harry Wasserman and his distinguished career in the field of heterocyclic compounds and organic synthesis.

Abstract

Oxidation of the guanine heterocycle by two electrons can yield the chiral product 5-carboxamido-5-formamido-2-iminohydantoin (**2Ih**). The **2Ih** free base enantiomers were synthesized from 2'-deoxyguanosine oxidized with a Cu(II)/H_2O_2 oxidant system followed by hydrolysis of the *N*-glycosidic bond. These isomers were each studied by electronic circular dichroism spectroscopy for determination of their absolute configurations. Time-dependent density functional theory calculations of the expected spectra were completed in both the gas phase and with solvent modeling in order to interpret the experimental spectra and provide the absolute configuration assignments.

Key words

Guanine Oxidation

2-Iminohydantoin

Electronic Circular Dichroism

Time-dependent Density Functional Theory

Introduction

Electron deficiency in DNA typically induces oxidation at the guanine base due to its low standard reduction potential.[1] Identification and characterization of the products resulting from oxidation of guanine, normally studied as 2'-deoxyguanosine nucleoside or in short oligomeric strands, have identified a diverse array of compounds.[2-6] Interestingly, some of these products introduce a stereocenter in what was once the planar achiral guanine base. Chiral guanine oxidation products are best exemplified by the hydantoins spiroiminodihydantoin (**Sp**) and 5-guanidinohydantoin (**Gh**, **Scheme 1**).[7-10] These chiral products exist as free base enantiomers, or diastereomers when attached to the 2-deoxyribose sugar. [11] The diastereomers of **dGh** provide a nearly impossible problem for determination of their absolute configurations, because they readily interconvert through an enolization reaction.[8] In contrast, **dSp** provided a challenging case for making assignments of its absolute configuration, because it only possesses exchangeable protons in the base. Studies aimed to define the (**d)Sp** absolute configuration by NMR,[12] optical rotatory dispersion,[13] and electronic circular dichroism (ECD),[14] all interpreted through quantum mechanical calculations, came to competing conclusions about the absolute configuration for **(d)Sp**. Further studies using vibrational circular dichroism and modeling of solvent in the ECD time-dependent density functional theory (TDDFT) calculations helped address the differing conclusions.[15] The **dSp** absolute configurations were solidified when an X-ray crystal structure for the *S* diastereomer was determined in a short oligodeoxynucleotide (ODN) crystallized in the active site of polymerase β.[11]

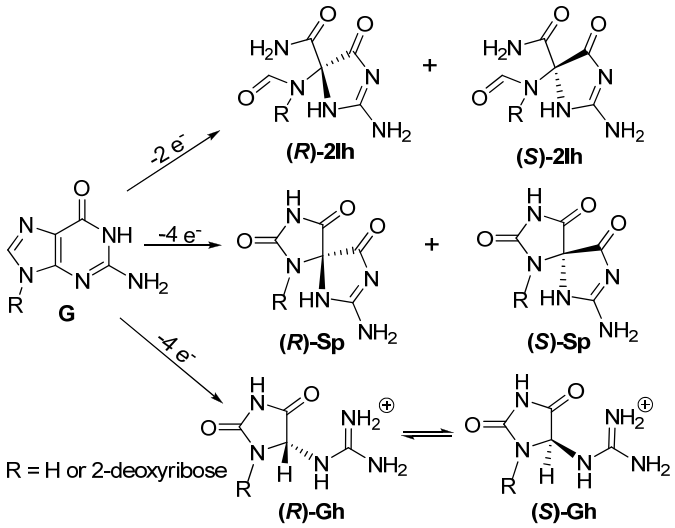

Scheme 1. Chiral products resulting from oxidation of the base of 2'-deoxyguanosine.

A third chiral product of guanine oxidation, referred to as 5-carboxamido-5-formamido-2-iminohydantoin-2'-deoxyribonucleoside, or **d2Ih**, also exists. This compound was first defined as having mass 34 units higher than the parent compound, and its structure was predicted based on chemical intuition;[16] further, a compound of the same mass was observed from oxidation of guanine in a ODN with a dinuclear copper(II) complex.[17] Subsequently, the structure for **d2Ih** was established by complementary NMR methods.[18] In addition, **d2Ih** has been observed during oxidation of 2'-deoxyguanosine by Mn-TMPyP/$KHSO_5$,[16,19] NiCR/$KHSO_5$,[20] dimethyldioxirane,[18] $Cu(OAc)_2/H_2O_2$,[21] $Pb(OAc)_2/H_2O_2$,[22] and $CO_3^{\bullet-}$.[23] These studies highlight **2Ih**, a two-electron oxidation product of guanine, as a possible primary oxidation product that might exist in the cellular context. However, **d2Ih** has not yet been observed in biological samples. Based on these findings, studies to understand the in vitro chemistry of **d2Ih** are underway. For interpretation of these results, it will be critical to know the absolute configuration for the **d2Ih** diastereomers.

In the present study, the **d2Ih** diastereomers were individually purified followed by cleaving the *N*-glycosidic bond in order to obtain the individual **2Ih** enantiomers. The ECD for each of the enantiomers was measured. TDDFT calculations were used to obtain predicted ECD spectra for the two enantiomers both in the gas phase and with solvent modeling; the predicted ECD spectra were then compared to the experimental spectra to assign their absolute configurations. Knowing the absolute configurations for the **2Ih** enantiomers allowed configurations of the **d2Ih** diastereomers in the nucleoside and ODN contexts to be assigned.

Results and discussion

Preparation of the **d2Ih** diastereomers was achieved through the $Cu(OAc)_2/H_2O_2$ reaction conditions developed in our laboratory.[21] The diastereomers were individually purified using a Hypercarb HPLC column and termed **d2Ih1** and **d2Ih2** based on their elution order. Their identities were initially determined by LC-ESI^+-MS (*m/z*: $[M+H]^+$ Calcd 302.3; Found 302.1; **Fig. S1**), as well as by ESI^+-MS/MS fragmentation of the free bases to obtain daughter fragments (*m/z*: $[M+H]^+$ = 186, 158, and 141) that were compared to literature values (*m/z*: $[M+H]^+$ = 186, 158, and 141; **Fig. S2**).[18] The **d2Ih** nucleosides exhibit free rotation about the *N*-glycosidic bond and a number of bonds in the base (**Scheme 2**); therefore, to simplify the interpretation of the experimental ECD spectra by TDDFT methods removal of the sugar by cleavage of the glycosidic bond was first conducted (**Scheme 2**). Removing the 2-deoxyribose sugar eliminates many atoms and one freely rotatable bond that would need to be addressed via quantum mechanical calculations. The purified nucleoside samples were incubated in HF/pyridine following literature protocols (40% HF 37 ºC for 90 min)[13] or in ddH_2O at 37 ºC for 48 h (**Fig. S3**). This study identified incubation in ddH_2O for 48 h at 37 ºC as a clean method for liberating the **2Ih**

enantiomers from the diastereotopic nucleosides. After purification of the individual **2Ih** enantiomers, spectroscopic studies were conducted.

The experimental ECD spectra recorded for **2Ih1** and **2Ih2** in ddH_2O were nearly mirror images of one another, as expected (**Fig. 1**). The spectra exhibited two lobes with a small rotation near 262 nm and larger rotation near 233 nm; more specifically, **2Ih1** gave a positive rotation at 262 nm and a negative rotation at 233 nm, while **2Ih2** had a negative rotation at 259 nm and a positive rotation at 231 nm.

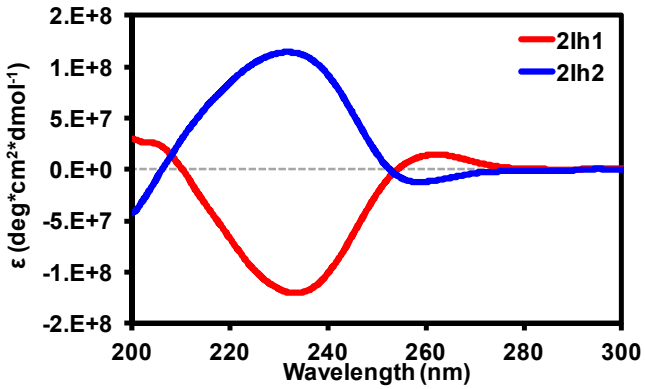

Figure 1. Experimental ECD spectra for the **2Ih** free base enantiomers. The spectra were recorded in ddH_2O at 20 °C on samples with ~0.15 mg mL^{-1} concentrations.

Before the TDDFT calculations of the expected ECD spectra could be completed, we first needed to explore the structure of **2Ih**. As the ring opening configuration without the sugar has not definitely been established there exist three possible constitutional isomers: ring opened with the formyl group at N9, ring closed, or ring opened with the formyl group at N7 (**Scheme 2**; the guanine numbering scheme was retained for clarity). Based on the energy minimization calculations for each of these three possible forms done under the conditions described in the experimental section, the lowest energy structure (> 10 kcal mol^{-1}) was identified to have the

formyl group at N9 (**Scheme 2, Fig. S4**). These results are in agreement with the structure proposed for the nucleosides based on NMR results, which also place the formyl group on N9.[18] Therefore, all further calculations on the **2Ih** enantiomers were completed on only this isomer.

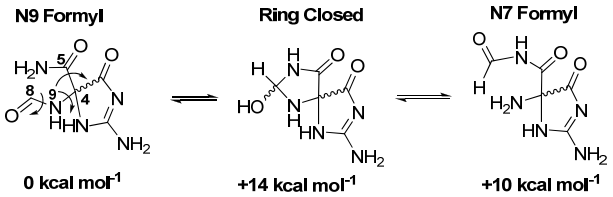

Scheme 2. Relative energies of the possible constitutional isomers of the **2Ih** free base.

In the N9 formyl isomer, there are three bonds, as indicated in **Scheme 2**, that can freely rotate leading to a series of rotamers that need to be understood computationally. Therefore, simultaneous dihedral scans about the N9,C4 and the C4,C5 bond angle at 20° increments were conducted on the *R* enantiomer to predict the energy as these bonds were rotated (**Scheme 2**), using the same conditions as the previous geometry optimizations. Independent dihedral scans of the N9,C8 bond were not conducted because it was left to freely rotate during the previous calculations. In the plots of energy versus the two bond angles for the enantiomer, the low energy conformations were selected (**Fig. S5**), and then submitted to a second round of optimization in which all bonds were allowed to freely rotate. From these calculations, four low energy structures emerged within 2.3 kcal mol^{-1} of the lowest energy structure (**Fig. 2**). The *S* enantiomer structures of these four were obtained by using the mirror invert function in Gaussview (v. 5.0) to ensure the rotamers were truly mirror images of the *R* enantiomer.

UU IR Author Manuscript

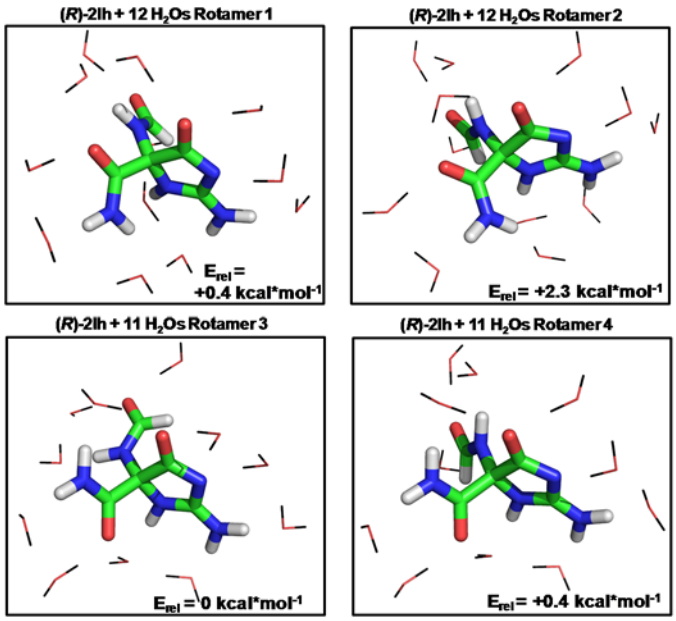

Figure 2. Rotamers for the **(*R*)-2Ih** enantiomer, shown along with the calculated positions of the waters in the first solvent shell. The reported relative energies were obtained on the structures without the added waters, as the presence of different numbers of waters did not allow an energy comparison of the hydrated structures.

The initial gas phase TDDFT calculations to predict the ECD spectra for the **2Ih** free base enantiomers were conducted on the four lowest energy rotamers found in the previous studies. The ECD spectrum for each rotamer was calculated under the conditions described in the experimental section. The ECD spectra were plotted from the excitation energies and the rotational lengths by overlapping the Gaussian functions for each transition.[15] Next, the computed ECD spectra for the rotamers were weighted using the Boltzmann distribution based on their calculated relative energies,[24] and then combined to produce the final calculated gas phase spectra shown in **Figure 3**. The overlap between the experimental and computed spectra for the enantiomers was good at the higher energy lobe (~232 nm), but at the lower energy lobe (~262 nm) the match between the two spectra was poorer than desired. The experimental and computed UV-vis spectra for the enantiomers also proved to give a poor overlap (**Fig. S6**). These results were good enough to make initial absolute configuration assignments for **2Ih1** and **2Ih2** as the *S* and *R* enantiomers,

respectively; however, these calculations did not reproduce all key features of the experimental spectra (**Fig. 3**). In our previous studies, the experimental ECD spectra for the **Sp** enantiomers were better reproduced when solvation was considered during the TDDFT calculations. Therefore, solvation modeling was included during the TDDFT simulation of the **2Ih** enantiomers.

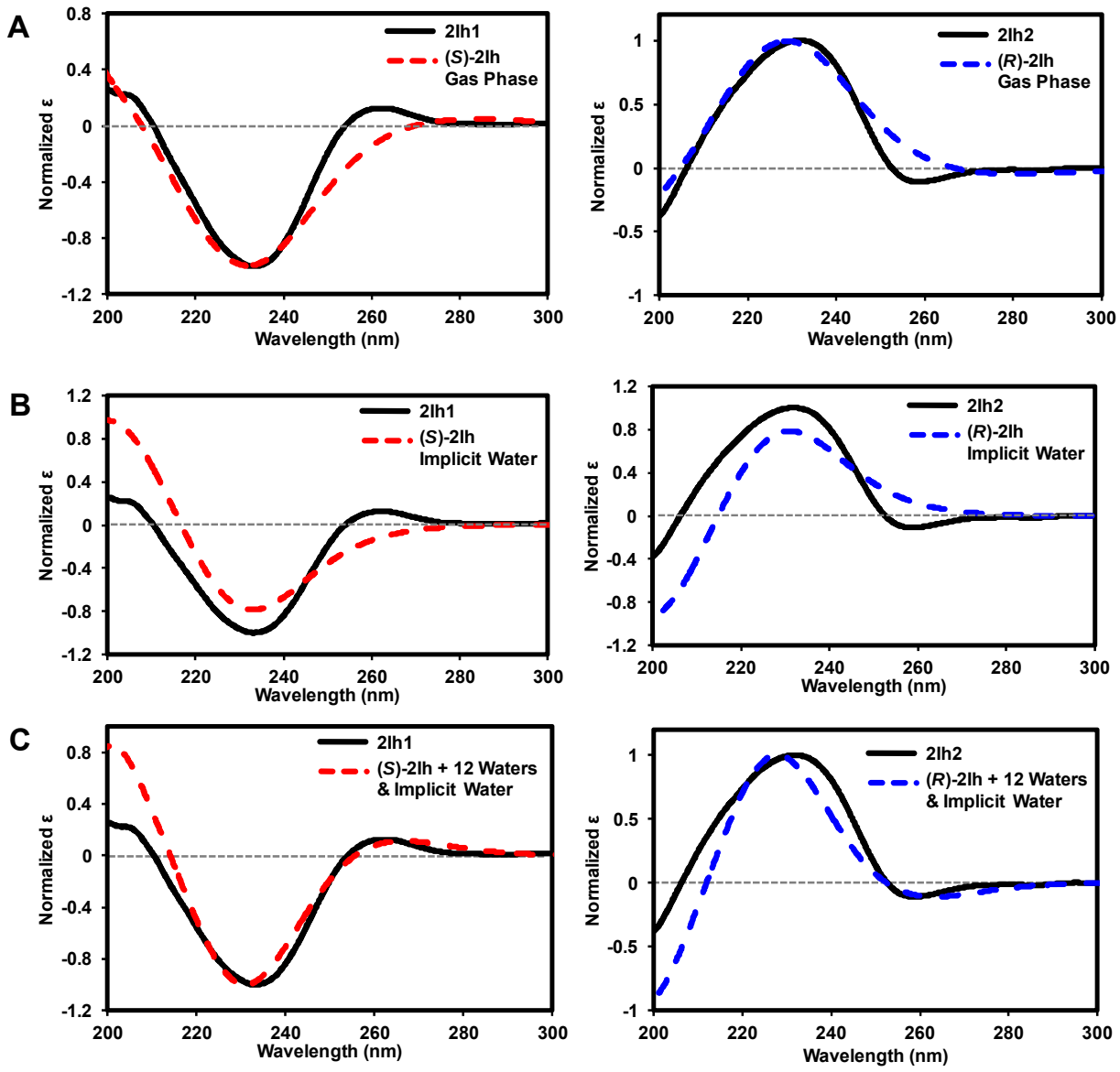

Figure 3. Comparison of experimental and theoretical ECD spectra for the **2Ih** enantiomers. (**A**) Comparison between gas phase calculations and the experimental spectra. To match experiment with theory, the gas phase theoretical spectra were blue-shifted by 10 and 13 nm for the *S* and *R* enantiomers, respectively. (**B**) Comparison between calculations that modeled solvation implicitly with the experimental data. To match experiment with theory the implicit solvation theoretical spectra were red-shifted by 4 and 2 nm for the *S* and *R* enantiomers, respectively. (**C**) Comparison between the implicit and explicit solvation modeled theoretical spectra and the experimental spectra. To match the experiment with theory fully solvated spectra were red-shifted by 7 and 4 nm for the *S* and *R* enantiomers, respectively.

Solvation was initially introduced to the TDDFT calculations using the polarizable continuum model (PCM) to add implicit solvation by water. The TDDFT simulations were

repeated with each rotamer including implicit water solvation and plotted as previously described. Comparison of the experimental and theoretical ECD spectra for each **2Ih** enantiomer gave a good prediction of the high energy lobe (~232 nm), but again failed to reproduce the low energy lobe (~262 nm) of the experimental spectra (**Fig. 3**). The overlap between the experimental and theoretical UV-vis spectra for the **2Ih** enantiomers were much closer when implicit solvation was introduced to the calculations (**Fig. S6**). These calculations again predict **2Ih1** to have the *S* configuration and **2Ih2** as the *R*. However, the overlap between the experimental and theoretical spectra left room for improvement.

Our previous ECD studies on the **Sp** enantiomers identified the need for adding explicit waters at all hydrogen bonding sites to the structures used in TDDFT calculations in order to obtain suitable agreement between experiment and theory.[15] This created the first hydration layer about the molecule. Therefore, the process of adding explicit solvation was repeated on the **2Ih** rotamers. Each optimized rotamer of both enantiomers was explicitly solvated with the first hydration layer and then the solvated structures were again optimized. This required either 11 or 12 waters, depending on the rotamer (**Fig. 2** and **Fig. S7**). Once optimized, these explicitly hydrated structures were used to run TDDFT simulations to predict the ECD spectra for each rotamer (**Fig. S8**). Next, the computed ECD spectra for the rotamers were weighted using the Boltzmann distribution based on their calculated relative energies from the dihedral scan calculations. The computed relative energies for the optimized solvated rotamers could not be used for weighting purposes because of the differing amounts of water molecules used for each one. The solvated calculations gave two lobes in the predicted ECD spectra similar to the experimental data (**Fig. 3**). The high energy lobe (~232 nm) matched the solvated calculation, and explicit solvation provided a lower energy lobe (~262 nm) that aligned with the experimental data. Lastly, the inclusion of

explicit and implicit solvation provided good overlap between the experimental and theoretical UV-vis spectra for the 2Ih enantiomers (**Fig. S6**). These solvated calculations again predicted **2Ih1** to be the *S* enantiomer and **2Ih2** to be the *R*. The overlap between experiment and theory for **(*S*)-2Ih** was good, while that for **(*R*)-2Ih** gave a broader high energy peak in the experiment than was predicted by theory (**Fig. 3**). This observation likely exists because the purified *R* enantiomer sample retained a small amount of the parent nucleoside (~10%, **Fig. S9**). The addition of nucleoside was not simulated in the theoretical calculations. Regardless of this small difference between experiment and theory, the assignments to establish the *R* and *S* enantiomers of **2Ih** are clear. Furthermore, the inclusion of explicit solvent modeling reproduced both lobes observed in the experimental ECD spectra for the **2Ih** enantiomers. Knowledge of the enantiomer absolute configurations allowed us to next address the assignments for the diastereomer peaks observed in the HPLC chromatograms for **d2Ih** in the nucleoside or ODN contexts.

The nucleoside **d2Ih** diastereomers are separable by Hypercarb HPLC and purification of these provided the source of the **2Ih** enantiomers after removal of the 2-deoxyribose sugar. The experimental spectrum for each **d2Ih** diastereomer was obtained and gave similar results as observed with the free bases (**Fig. S10**). Assuming the inclusion of the 2-deoxyribose sugar does not perturb the equilibrium between the three possible base configurations (**Scheme 2**), which would impact the TDDFT calculations, the nucleoside diastereomer **d2Ih1** has the *S* configuration and **d2Ih2** has the *R* configuration. The only other context in which the **d2Ih** configurations are not yet established is in the context of a short ODN.

To address the elution order for the *R* and *S* **d2Ih** isomers in an ODN they were synthesized, individually purified, digested to nucleosides, and analyzed by Hypercarb HPLC to identify the stereochemistry of the **d2Ih** nucleoside liberated from the ODN. Synthesis of **d2Ih** in an ODN

was achieved using NiCR/$KHSO_5$ as previously reported by our laboratory in the strand 5'-AAT CCA C**X**A CAC CTC-3' where **X** = **d2Ih** diastereomers.[20] The **d2Ih**-containing ODNs were purified on an ion-exchange HPLC column (Dionex DNApac PA100) to obtain diastereomerically pure ODNs. Confirmation of **d2Ih** in the ODN was obtained by ESI^+-MS on a sample that contained a mixture of the diastereomers (Mass Calcd 4497.7; Found 4498.2). The liberated nucleosides from nuclease and phosphatase digestion of the diastereomerically pure **d2Ih**-containing ODNs were analyzed by Hypercarb HPLC to identify the diastereomer elution profile. These results revealed that the first eluting **d2Ih** diastereomer in the ODN context digested down to the first eluting diastereomer (*S*) on the Hypercarb column, and the second eluting **d2Ih** diastereomer in the ODN context digested down to the second eluting diastereomer (*R*) on the Hypercarb column (**Fig. 4**). Additionally, the **d2Ih** nucleosides slightly hydrolyzed to liberate the **2Ih** free bases during the digestion reactions, in which the enantiomers co-elute in between the nucleoside diastereomers. The presence of the free base in each sample provided a perfect peak for calibration to ensure the elution order of the diastereomers. These results will be critical for future studies aimed at addressing all diastereoselective reactions these isomers will be tested on.

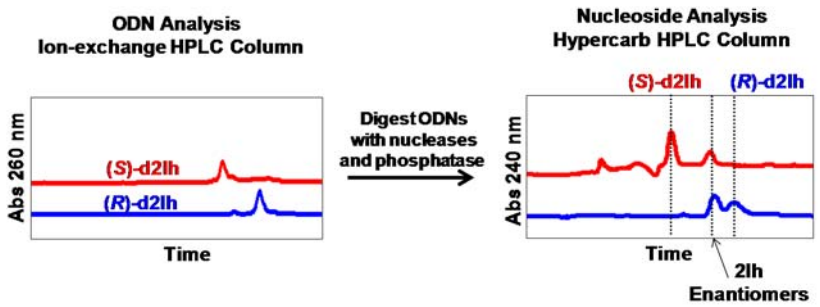

Figure 4. Order of elution for the **d2Ih** diastereomers in the ODN context (top) and nucleoside context (bottom). The ODN 5'-AAT CCA C**X**A CAC CTC-3' had **d2Ih** synthesized at position **X** with NiCR/$KHSO_5$ via a literature protocol from our laboratory.[20] After purification of the individual diastereomers embedded in the ODN they were digested with a suite of nucleases and phosphatase to nucleosides that were analyzed by Hypercarb HPLC to identify the stereochemistry of **d2Ih** in the ODN context.

With knowledge of the HPLC elution profile for the **d2Ih** diastereomers a comparison of the present results can be made to those found for the **dSp** diastereomers. Because the ECD spectra for the **2Ih** free base enantiomers and **d2Ih** nucleoside diastereomers are the same (**Fig. S10**), it was concluded that the first **d2Ih** eluting isomer from a Hypercarb HPLC column has the *S* configuration and the second has the *R* configuration. In our previous studies, the same type of analysis was used to assign the absolute configurations for the **Sp** enantiomers and **dSp** diastereomers. These studies revealed that on the Hypercarb HPLC column **(*R*)-dSp** elutes first and **(*S*)-dSp** elutes second. In contrast, the elution order for the **d2Ih** nucleoside diastereomers on the Hypercarb HPLC column identified *S* to elute first and *R* second. The second HPLC elution profile to compare **d2Ih** and **dSp** is on the elution order of the diastereomers in an ODN from an ion-exchange HPLC column. In the current studies, the **d2Ih** diastereomers embedded in a 15-mer ODN eluted from an ion-exchange HPLC column with *S* first and *R* second, which is similar to the profile observed in the nucleosides. In contrast, the **dSp** diastereomers in an ODN elute with the *S* isomer first and *R* second that is the opposite order observed on the Hypercarb HPLC column for the nucleosides and is consistent with other literature reports.[15,25] These observations support the physical difference between the *R* and *S* isomers for **d2Ih** and **dSp** effecting their HPLC elution order are not solely determined by stereochemistry. Also, **dSp** provides a special case because its isomer-dependent elution profile switches between HPLC columns, and the

UU IR Author Manuscript

inclusion of explicit solvation is required for prediction of its ECD spectra; both of these differences were not observed with **d2Ih**.

Conclusions

The present studies identified the absolute configurations for the **2Ih** enantiomers via ECD analysis of the free bases interpreted via TDDFT calculations with the aid of added solvation modeling. The role of explicit solvation in modeling the ECD spectra for chiral molecules by TDDFT has emerged as an important parameter that assists in obtaining satisfactory agreement between experiment and theory. The current results provide another example in which solvation was beneficial, however, not required, unlike the case of **Sp** from our previous studies.[15] Modeling of solvation adds to the complexity of the calculations and is likely not the first step to consider during TDDFT simulation of ECD spectra; though, for example, **Sp**,[15] and methyloxirane[26] required explicit solvation to obtain suitable assignment of absolute configurations consistent between experiment and theory. Further, ECD spectra prediction by TDDFT calculations provides a suitable method to assigning absolute configurations for chiral molecules that may or may not require consideration of solvation in the absence of an x-ray crystal structure.

Experimental

Synthesis of the **d2Ih** nucleoside diastereomers was achieved using Cu(II)/H_2O_2 and *N*-acetylcysteine following literature protocols.[21] Purification of the diastereomers was performed on a Hypercarb HPLC column (150 X 4.6, 5 μm). The purified **d2Ih** diastereomers were incubated in ddH_2O for 48 h at 37 °C to effect hydrolysis of the *N*-glycosidic bond to obtain the **2Ih** free base enantiomers that were individually purified using the same HPLC column. ECD spectra for the diastereomers and enantiomers were measured in ddH_2O at 20 °C on samples with a concentration

of 0.15 mg mL^{-1}, and the value for the **2Ih** extinction coefficient was previously reported.[21] Synthesis of **d2Ih** in an ODN was achieved using NiCR/$KHSO_5$ via a literature protocol.[20] Digestion of the purified **d2Ih**-containing ODNs was effected using snake venom phosphodiesterase, nuclease P1, and calf intestinal phosphatase following literature methods.[21] The liberated **d2Ih** nucleoside was analyzed using the previously described method. Full experimental details can be found in the supporting information file.

All calculations were done using the Gaussian 09 software package.[27] Geometry optimizations and dihedral scans were completed using the B3LYP functional[28,29] with the 6-311G[30,31] basis set while using the polarizable continuum model (PCM)[32,33] to implicitly define the solvent as water. The explicit solvation was completed by adding a water molecule to each hydrogen bonding site on the molecule, followed by a complete geometry optimization at the same level of theory used on the optimization of the single molecule. The ECD spectrum for each rotamer was calculated using the M06-2X functional[34] and 6-311++G(2d,2p) basis set, with the number of states (singlet only) set to 25. The ECD spectra were plotted from the excitation energies and the rotational lengths by overlapping the Gaussian functions for each transition, while using a line broadening factor = 3000 cm^{-1}.[15] Next, the computed ECD spectra for the rotamers were weighted using the Boltzmann distribution based on their calculated relative energies and then combined to produce the final calculated spectra.[24]

Acknowledgments

This work was supported by an NIH grant (CA090689). Computational resources from the Center for High Performance Computing at the University of Utah are gratefully acknowledged.

Supplementary material

Supplementary data (synthetic procedures, LC-ESI$^+$-MS, ESI$^+$-MS/MS, and coordinates for quantum mechanical calculations) associated with this article can be found, in the online version, at http://dx.doi.org/10.1016/j.tetlet.2014.12.052.

References

(1) Steenken, S.; Jovanovic, S. V. *J. Am. Chem. Soc.* **1997**, *119*, 617-618.
(2) Burrows, C. J.; Muller, J. G. *Chem. Rev.* **1998**, *98*, 1109-1152.
(3) Cadet, J.; Wagner, J. R.; Shafirovich, V.; Geacintov, N. E. *Int. J. Radiat. Biol.* **2014**, *90*, 423-432.
(4) Gimisis, T.; Cismas, C. *Eur. J. Org. Chem.* **2006**, *2006*, 1351-1378.
(5) Delaney, S.; Jarem, D. A.; Volle, C. B.; Yennie, C. J. *Free Radical Res.* **2012**, *46*, 420-441.
(6) Pratviel, G.; Meunier, B. *Chem. Eur. J.* **2006**, *12*, 6018-6030.
(7) Luo, W.; Muller, J. G.; Rachlin, E. M.; Burrows, C. J. *Org. Lett.* **2000**, *2*, 613-616.
(8) Ye, Y.; Muller, J. G.; Luo, W.; Mayne, C. L.; Shallop, A. J.; Jones, R. A.; Burrows, C. J. *J. Am. Chem. Soc.* **2003**, *125*, 13926-13927.
(9) Crean, C.; Geacintov, N. E.; Shafirovich, G. V. *Angew. Chem., Int. Ed.* **2005**, *44*, 5057-5060.
(10) Sugden, K. D.; Campo, C. K.; Martin, B. D. *Chem. Res. Toxicol.* **2001**, *14*, 1315-1322.
(11) Eckenroth, B. E.; Fleming, A. M.; Sweasy, J. B.; Burrows, C. J.; Doublie, S. *Biochemistry* **2014**, *53*, 2075-2077.
(12) Karwowski, B.; Dupeyrat, F.; Bardet, M.; Ravanat, J. L.; Krajewski, P.; Cadet, J. *Chem. Res. Toxicol.* **2006**, *19*, 1357-1365.
(13) Durandin, A.; Jia, L.; Crean, C.; Kolbanovskiy, A.; Ding, S.; Shafirovich, V.; Broyde, S.; Geacintov, N. E. *Chem. Res. Toxicol.* **2006**, *19*, 908-913.
(14) Ding, S.; Jia, L.; Durandin, A.; Crean, C.; Kolbanovskiy, A.; Shafirovich, V.; Broyde, S.; Geacintov, N. E. *Chem. Res. Toxicol.* **2009**, *22*, 1189-1193.
(15) Fleming, A. M.; Orendt, A. M.; He, Y.; Zhu, J.; Dukor, R. K.; Burrows, C. J. *J. Am. Chem. Soc.* **2013**, *135*, 18191-18204.
(16) Vialas, C.; Claparols, C.; Pratviel, G.; Meunier, B. *J. Am. Chem. Soc.* **2000**, *122*, 2157-2167.
(17) Li, L.; Murthy, N. N.; Telser, J.; Zakharov, L. N.; Yap, G. P. A.; Rheingold, A. L.; Karlin, K. D.; Rokita, S. E. *Inorg. Chem.* **2006**, *45*, 7144-7159.
(18) Ye, W.; Sangaiah, R.; Degen, D. E.; Gold, A.; Jayaraj, K.; Koshlap, K. M.; Boysen, G.; Williams, J.; Tomer, K. B.; Mocanu, V.; Dicheva, N.; Parker, C. E.; Schaaper, R. M.; Ball, L. M. *J. Am. Chem. Soc.* **2009**, *131*, 6114-6123.
(19) Tomaszewska, A.; Mourgues, S.; Guga, P.; Nawrot, B.; Pratviel, G. *Chem. Res. Toxicol.* **2012**, *25*, 2505-2512.

(20) Ghude, P.; Schallenberger, M. A.; Fleming, A. M.; Muller, J. G.; Burrows, C. J. *Inorg. Chim. Acta* **2011**, *369*, 240-246.
(21) Fleming, A. M.; Muller, J. G.; Ji, I.; Burrows, C. J. *Org. Biomol. Chem.* **2011**, *9*, 3338-3348.
(22) Banu, L.; Blagojevic, V.; Bohme, D. K. *J. Phys. Chem. B* **2012**, *116*, 11791-11797.
(23) Rokhlenko, Y.; Geacintov, N. E.; Shafirovich, V. *J. Am. Chem. Soc.* **2012**, *134*, 4955-4962.
(24) Pipolo, S.; Percudani, R.; Cammi, R. *Org. Biomol. Chem.* **2011**, *9*, 5149-5155.
(25) Khutsishvili, I.; Zhang, N.; Marky, L. A.; Crean, C.; Patel, D. J.; Geacintov, N. E.; Shafirovich, V. *Biochemistry* **2013**, *52*, 1354-1363.
(26) Mukhopadhyay, P.; Zuber, G.; Goldsmith, M. R.; Wipf, P.; Beratan, D. N. *ChemPhysChem* **2006**, *7*, 2483-2486.
(27) Frisch, G. W. e. a., *Gaussian 09*, revision C.01; Gaussian, Inc.: Wallingford, CT, 2010.
(28) Becke, A. D. *J. Chem. Phys.* **1993**, *98*, 5648-5652.
(29) Lee, C.; Yang, W.; Parr, R. G. *Phys. Rev. B* **1988**, *37*, 785-789.
(30) Krishnan, R.; Binkley, J. S.; Seeger, R.; Pople, J. A. *J. Chem. Phys.* **1980**, *72*, 650-654.
(31) Frisch, M. J.; Pople, J. A.; Binkley, J. S. *J. Chem. Phys.* **1984**, *80*, 3265-3269.
(32) Scalmani, G.; Frisch, M. J. *J. Chem. Phys.* **2010**, *132*, 114110.
(33) Tomasi, J.; Mennucci, B.; Cammi, R. *Chem. Rev.* **2005**, *105*, 2999-3093.
(34) Zhao, Y.; Truhlar, D. *Theor. Chem. Acc.* **2008**, *120*, 215-241.